Carbon nanotubes as conducting support for potential Mn-oxide electrocatalysts: influences of pre-treatment procedures

Saskia Buller[a,*], Marius Heise-Podleska[a], Norbert Pfänder[a], Marc Willinger[a], Robert Schlögl[a,b]

[a]*Max Planck Institute for Chemical Energy Conversion, Stiftstraße 34-36, 45470 Mülheim an der Ruhr, Germany*

[b]*Fritz Haber Institute of the Max Planck Society, Faradayweg 4-6, 14195 Berlin, Germany*

Article history:

Received 9 December 2015

Revised 6 January 2016

Accepted 7 January 2016

Available online

Abstract

Different oxygen and nitrogen containing functional groups were created on the surface of the multi-walled carbon nanotubes. The multi-walled carbon nanotubes were treated in ultra sonic bath with sulfuric or nitric acid. Furthermore the surface texture was modified by increase of the roughness. In particular after treatment with the oxidizing nitric acid, in comparison to the H_2SO_4 or ultra-sonic treated samples, craters and edges are dominating the surface structures. Manganese oxide was deposited on the multi-walled carbon nanotubes by precipitation mechanism. Various manganese oxides are formed during the deposition process. The samples were characterized by elemental analysis, microscopy, thermal analysis, Raman spectroscopy, and by the zeta potential as well as X-ray diffraction measurements. It was shown that the deposited manganese oxides are stabilized rather by surface texture of the multi-walled carbon nanotubes than by created functional groups.

Key words: Multi-walled carbon nanotubes (MWCNT); Surface modification; Raman spectroscopy; Manganese deposition; Zeta potential

*** Corresponding author.** Tel: +49 208 3063701; Fax: +49 208 3063951; E-mail:

saskia.buller@cec.mpg.de.

1. Introduction

The energy challenge is a major project for today's society. Storage of energy can be fulfilled by the conversion of electricity into chemical energy carriers like hydrogen. The electrolysis of water requires catalytic active and stable electrode materials, which are currently platinum, iridium oxide or ruthenium oxides [1,2]. For global applications the expensive noble rare metals have to be replaced by alternative abundant materials like compounds of carbon and manganese oxides, which are promising candidates [3]. Stability while maintaining high activities of the materials is hereby a major challenge. Research with the focus on stabilization effects is required for a detailed understanding of corrosion during the electrolysis.

Carbon nanotubes (CNT) contain several interesting properties making these materials suitable for many applications. Due to their high specific surface area of about 250 m^2/g their utilization as support materials for organic molecules or inorganic particles for catalytic purposes is excellent [4,5]. Organic linkers can be attached to the surface of the CNT by a covalent bonding through various sidewall reactions as well via noncovalent Van-der-Waals interactions [6]. Adsorption of metal nanostructures is based on attractive Van-der-Waals and repulsive forces as described by the DLVO (Derjaguin-Landau-Verwey-Overbeek) theory. Hereby the metal particles and the carbon surface are considered as capacitors. According to this concept of interactions between charged particles, it is obvious that a chemical treatment of the involved surfaces has a critical impact on the deposition effects. Particularly if one considers that only accessible active sites on the surface can contribute to the catalyst activity [7].

Multi-walled carbon nanotubes (MWCNT) are built of several cylinders, which are stacked into one another. Each cylinder consists of sp^2 hybridized carbon sheets, equivalent to rolled-up graphene. The connectivity of the ends of the graphene sheets defines the two possible orientations, namely armchair or zigzag, respectively. The electronic properties make CNT very versatile as conductive support materials for electrodes in electrocatalysis [3]. Surface functional groups as well as defects in the outer layer of the MWCNT dominantly affect its properties. Modifications of the surface can be performed by gaseous or liquid treatment [8,9,10]. The morphology of the samples treated in gas phase thereby remains nearly

unaffected [11]. The modified material properties show an improved performance in catalytic applications [12] or provide anchoring groups for the deposition of metal particles [13]. Depending on the treatment method, different types of functional groups can be created. By liquid nitric acid treatment more carboxylic, anhydride and hydroxyl groups are formed, while by gaseous phase (5% O_2 in N_2) treatment more carbonyl and quinone groups are formed [14].

Manganese oxides exist in various oxidation states, and within the states in different structures like α-, β-, δ-MnO_2, or as amorphous phase. They are studied as electrocatalysts for water splitting, as anode for oxygen evolution reaction (OER) and, furthermore, as cathode for oxygen reduction reaction (ORR) [15,16]. In comparison to commonly used noble metal-based catalysts like platinum, palladium, iridium oxides, or ruthenium oxides, manganese oxides are inexpensive, natural abundant and environmental friendly. It was reported that the total oxidation of ethyl acetate by a dynamic mechanism including Mn^{4+} and Mn^{3+} oxide occur, which leads to the conclusion that Mn-oxides are active in manipulating the oxygen molecule chemistry. Further, manganese oxides are also known to be active materials for capacitors [17,18]. An enhancement of the capacitance of pure graphene by a factor of three up to 310 F/g was reported, caused by manganese oxide deposition [19].

Both components, carbon and manganese oxides are interesting materials for electrocatalysis. The combined dual functions of charge carrier transport and redox activities of oxygen are the relevant properties here. In order to define a structure-function relation, a first understanding of the chemical interaction between the metal oxide and the MWCNT surface is needed. In this work, we study the influence of different treatment methods on MWCNT and their stabilization effects on deposited manganese oxides. Investigations were performed with increasing quantities of deposited manganese.

2. Experimental

2.1. Cleaning and pre-functionalization of MWCNT

MWCNT produced by Shandong Dazhang Nano Materials Co. were separated in three batches. For the reaction with nitric or sulfuric acid, in each case 20 g of MWCNT were mixed with 500 mL of acid, stirred and heated up under reflux at around 100 °C for 16 h (H_2SO_4) or 3 h (HNO_3). After the reaction the gaseous supernatant was purged with nitrogen to remove acidic vapor for better handling. The material was filtered and washed extensively in a washing cell over night with distilled water to remove residual acid and impurities like iron which initial amount is reduced by these acid treatments by around

two third. The third batch counts as reference for pure MWCNT. Treatment in ultra-sonic bath for two hours at room temperature was applied to remove amorphous carbon from the surface as described in literature [20].

2.2. Impregnation of MWCNT with manganese (II)

The pre-functionalized MWCNT were divided into portions of 1.9 g each, and then wetted with distilled water to fill the inner channels of the carbon nanotubes. This favors a deposition on the outer surface of the MWCNT, following the selective deposition described in literature [21]. To obtain different loadings of manganese on each portion of the MWCNT, 20 mL of manganese (II) nitrate tetrahydrate ($Mn(NO_3)_2 \cdot 4H_2O$, Merck) solutions with increasing concentrations of 0.06 mol/L, 0.12 mol/L, and 0.18 mol/L, were added dropwise under stirring. For the loading of the ultra-sonic bath treated samples concentrations of 0.018 mol/L, 0.09 mol/L, and 0.18 mol/L were used. The pH value was kept constant at pH 8. The products were dried at 60 °C for 6 h and afterwards at 110 °C for 24 h in air.

2.3. Elemental analysis

The elemental analysis was executed by the external analysis laboratory Kolbe (Höhenweg 17, 45470 Mülheim an der Ruhr, Germany), using a Vario EL CHNOS-Analyzer from elementar company.

2.4. N_2 sorption measurements

N_2 sorption measurements were performed with an Autosorb6 (Quantachrome) at 77 K. The samples were outgassed for 2 h at 110 °C. The evaluation of the data was done by BET theory.

2.5. Microscopy

STEM Microscopy images were taken by a Cs corrected Hitachi HD-2700 STEM with a cold field emission gun and an accelerating voltage of 200 kV, equipped with an EDAX Octane T Ultra W EDX (energy dispersive X-ray) detector. HAADF and corresponding annular bright field STEM images were recorded using a double Cs corrected JEOL ARM microscope with a cold field emission gun. The instrument was operated at 200 kV.

2.6. Thermal anaylsis

Thermoanalytic analyses were performed with a NETSCH STA449F3 thermobalance setup connected to a quadrupole mass spectrometer (MS) QMS 403 D from Aëolus. Measurements were taken in Ar atmosphere with a constant gas flow of 50 mL/min in a temperature range of 40–1000 °C with a heating

rate of 20 K/min. The corundum ceramic crucibles were filled with approximately 20 mg of sample material for the measurements.

2.7. Zeta potential

Zeta potentials were measured by a ZetaPALS90 analyzer from Brookhaven Instruments Corporation, equipped with an autotitrator. The principle of phase analysis light scattering (PALS) to determine the electrophoretic mobilities exhibits a 100 times higher precision than measurements by Doppler shift as described in detail in literature [22]. The phase shift was measured using a 639 nm laser, whereas the current of the cell was automatically adjusted at around 2 mA. 20 mL of the dissolved sample was dispersed in an ultra-sonic bath for 5 min and analyzed within a range of pH 10 to pH 2 adjusted by drops of NaOH and HNO_3.

2.8. Raman spectroscopy

Raman spectra were measured using a Thermo Scientific DXR Raman Microscope with a 50x magnification and a 532 nm laser. The samples were measured for 2 s and an exposure rate of 2 with a laser power of 3 mW. The fitting procedure is described in detail in literature [23]. Briefly, two defect peaks (D, D') and one graphitic peak (G) were fitted to determine their percentage of the framework of the MWCNT. The D*/G ratio corresponds to the degree of defect sites calculated by the peak areas of the total sum of D- and D'-bands and the ideal graphitic band.

2.9. X-ray diffraction (XRD)

X-ray diffraction patterns were recorded in Bragg-Brentano geometry on a Bruker AXS D8 Advance theta/theta diffractometer, using Ni filtered Cu *K*α radiation and a position sensitive LynxEye silicon strip detector.

3. Results and discussion

3.1. Effect of pre-treatment on MWCNT

Thermal analysis displays temperature depending decomposition of the material, which leads to the identification of different functional groups. Gravimetric measurements point to the amount of functional groups. The total mass loss of the MWCNT pre-treated with nitric acid is more pronounced than for sulfuric acid or even less for ultra-sonic bath treated samples as seen in Figure 1. Considering the specific masses (Figure 2) that were detected during the decomposition of the materials in dependence of

temperature, it is possible to distinguish between different functional groups. As known from literature [14] the presence of CO_2 (44 amu) in a temperature range of 100–450 °C corresponds to carboxylic groups as seen for the nitric acid treated sample and slightly for the sulfuric acid treated sample. The carboxylic groups created on the surface of the MWCNT are less stable, due to occurrence at around 300 °C. Additional lactone groups have been detected for the nitric acid treated sample due to the occurrence of CO_2 at higher temperatures in-between 550 and 800 °C. Anhydrides can be identified by the common release of CO (28 amu) and CO_2 seen for the nitric acid sample and faintly visible for the sulfuric acid treated sample. A mass peak of NO (30 amu) was found for the nitric acid treated sample. This indicates nitrate groups or rather physisorbed HNO_3 due to the release at low temperatures caused by remaining acid although the samples were washed extensively with distilled water. Water peaks are detected for the sulfuric and nitric acid treated samples at low temperatures. These peaks are caused by water physisorbed at functional groups or inner channels that became accessible due to opening of the ends of the MWCNT from acid treatment [24]. Overall, the nitric acid treated sample contains various oxygen functional groups on the surface, while the sulfuric acid treated sample contain only minor functional groups. The MWCNT pre-treated in an ultra-sonic bath do not contain functional groups that could be determined by thermal analysis. Zeta potential measurements confirm the results determined by thermal analysis (Figure 3). The samples pre-treated in ultra-sonic bath, containing no functional groups on the surface, exhibit zeta potentials around zero mV. Negative zeta potentials are present for the acid treated samples, significantly more distinct for the nitric acid treated sample than for the sulfuric acid treated sample.

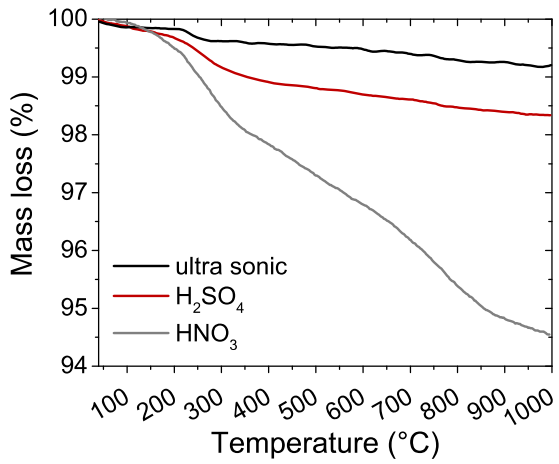

Figure 1. Mass loss of different pre-treated MWCNT in dependence of temperature between 40–1000 °C measured with a heating rate of 20 K/min.

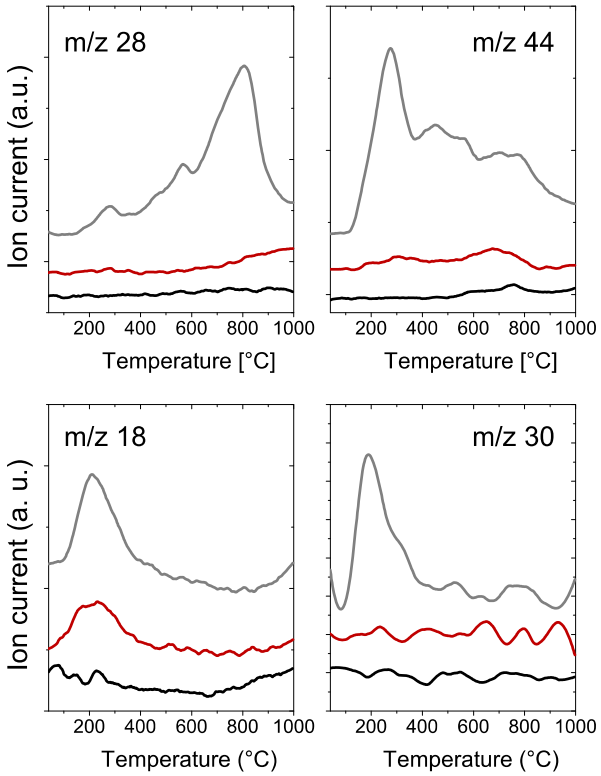

Figure 2. MS signals of thermal analysis experiments on ultra-sonic (black), sulfuric acid (red) and nitric acid (grey) treated MWCNT.

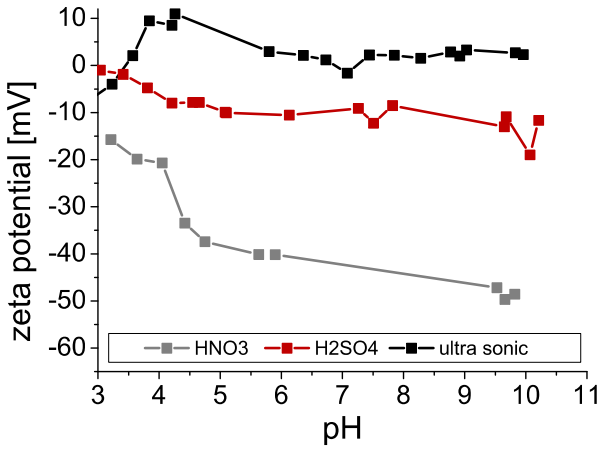

Figure 3. Zeta potential measurements of different pre-treated multi-walled carbon nanotubes.

Microscopy images reveal the surface structures of the MWCNT, which differ significantly depending on the pre-treatment method, partial amorphization of the surface can be observed. Nitric acid pre-treated samples show pronounced defects in the outer surface seen by images recorded with secondary electrons (Figure 4b). Damages look like crater on the surface, forming distinct edges and

providing possible anchoring points for metal deposition. The pre-treatment with sulfuric acid leaves the surface of the MWCNT mainly intact (Figure 4a).

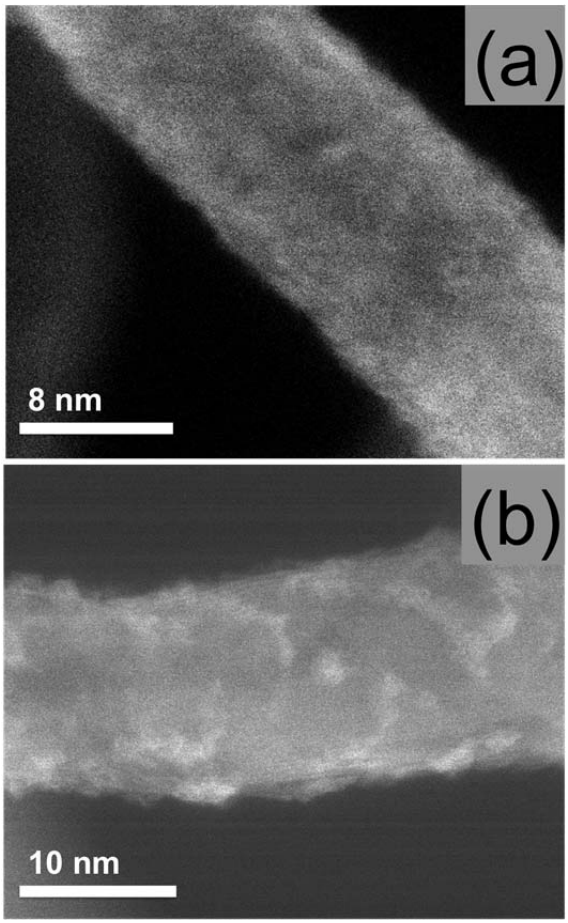

Figure 4. Microscopy images of sulfuric (a) and nitric acid (b) pre-treated MWCNT in secondary electron mode.

Raman spectroscopy is a central method to characterize the bulk structure of the carbon materials. Regarding the so-called G-band which is induced by resonance Raman scattering in an ideal graphitic sp^2 material, contrasting the D- and D'-bands which are induced by phonon scattering processes in a non-defect free lattice. It is a very sensitive method to detect changes in the ideal graphitic layers of MWCNT induced by chemical treatment. With the fitting procedure described in literature it is even possible to distinguish between different treatment methods [23]. The D*/G ratios determined by the peak areas of the D, D' and G peaks shows that more defects are formed within the graphite lattice with nitric acid than with sulfuric acid, verifying the observations made by thermal analysis, zeta potential measurements and microscopy (Figure 5). MWCNT treated in an ultra-sonic bath have the lowest D*/G

ratio with the highest amount of ideal graphitic lattice.

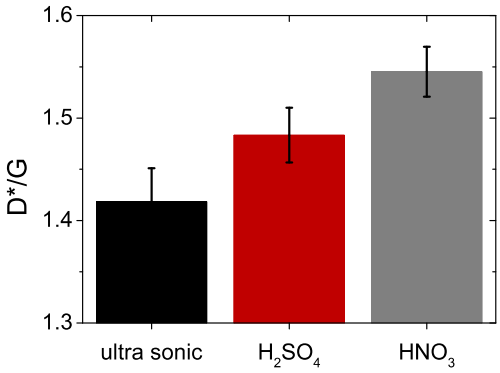

Figure 5. D*/G ratio determined by the peak areas of D, D' and G bands. The nitric acid pre-treated sample has the highest defect ratio.

3.2. Manganese deposition

The deposited amount of manganese rises linearly with increasing concentration of added manganese (II) solution as summarized in Table 1. This indicates a deposition precipitation loading mechanism. Thus, we expect a particulate nature of the Mn species rather than a molecular ion-exchange. The samples are henceforth named in accordance to the deposited amount of manganese. Nitrogen contents in the samples tend to be high due to remaining nitrate ions of the manganese(II)nitrate solutions and from physisorbed nitrogen on the surface from purging process. Differences of the added amount of manganese are related to differences in specific surface areas determined with N_2 sorption measurements and evaluated by BET theory. The specific surface areas increase after pre-treatment with sulfuric acid and more pronounced after pre-treatment with nitric acid caused by the effect of opening of the ends of the MWCNT [24]. As seen in Figure 6, the specific surface area decreases immensely after impregnation with manganese (II) solution, due to filling of inner channels of the MWCNT. To get a further insight into the composition of the synthesized materials, the molar ratios Mn to O were calculated and plotted in Figure 7. With increasing amount of deposited manganese the ratio decreases, following various manganese oxides are present. The Mn to O ratios of the ultra-sonic treated samples are close to 2, indicating that MnO_2 is present, confirming the considerations of the precipitation loading mechanism.

The ratios of the acid pre-treated samples are generally higher due to the fact that there is additional oxygen present from the functional groups.

Table 1. Results from elemental analysis and specific surface areas of N_2 sorption measurements using BET theory. Oxygen was determined indirectly by subtraction of the C, H, N and Mn content from 100 %.

Sample name	C (wt%)	H (wt%)	N (wt%)	Mn (wt%)	O (wt%)	BET surface area (m^2/g)	Sample number
Ultra-sonic	98.34	0.68	0.13		0.85	237	20437
1 wt%	95.42	0.16	0.32	1.56	2.54	244	21627
6 wt%	89.28	0.08	0.37	6.37	3.90	220	21628
11 wt%	81.55	0.06	0.28	10.76	7.35	215	21629
H_2SO_4	98.23	0.73	0.32		0.72	247	21980
1 wt%	95.63	0.33	0.35	0.94	2.75	234	21981
4 wt%	90.73	0.49	0.13	4.00	4.65	219	21982
6 wt%	84.66	0.30	0.62	6.53	7.89	219	21983
HNO_3	95.26	0.36	0.28		4.10	279	21976
1 wt%	90.96	0.38	0.55	1.65	6.46	236	21977
4 wt%	85.00	0.79	0.40	4.79	9.02	217	21978
6 wt%	83.99	0.81	0.79	6.92	7.49	206	21978

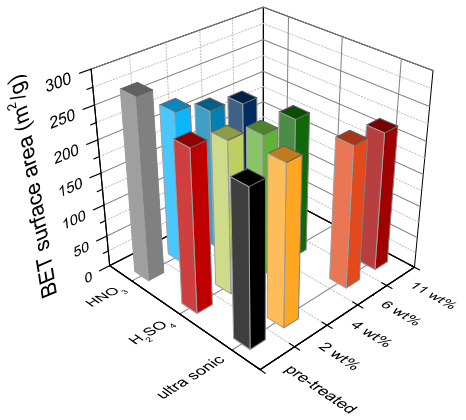

Figure 6. Specific surface areas determined with N_2 sorption and evaluation by BET theory for ultra-sonic (black), H_2SO_4 (red) and HNO_3 (grey) and corresponding impregnated MWCNT as labeled.

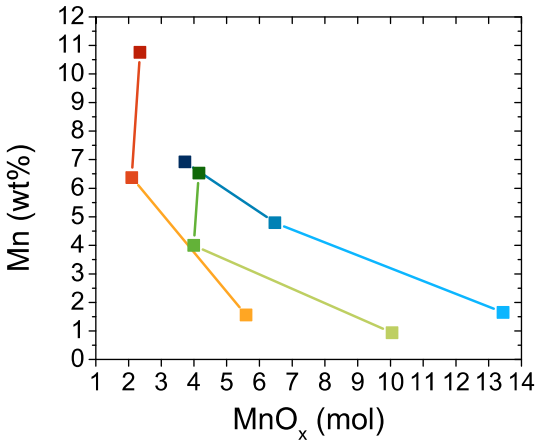

Figure 7. Molar ratios of oxygen related to one mol of manganese for the impregnated samples pre-treated with ultra-sonic bath (red), nitric (blue) or sulfuric acid (green).

Thermal analysis of the manganese loaded samples clarifies that the decomposition of the carbon support material starts at lower temperatures with increasing amount of manganese and increasing amount of functional groups seen by earlier release of CO and CO_2 (Figure 8). NO from remaining manganese(II) nitrate tetrahydrate from manganese deposition procedure is released at around 200 °C. The mandatory calcination process for applying these materials as electrodes has to be fulfilled due to the dependence of pre-treatment and manganese loading in a very careful way and was consequently omitted for this study.

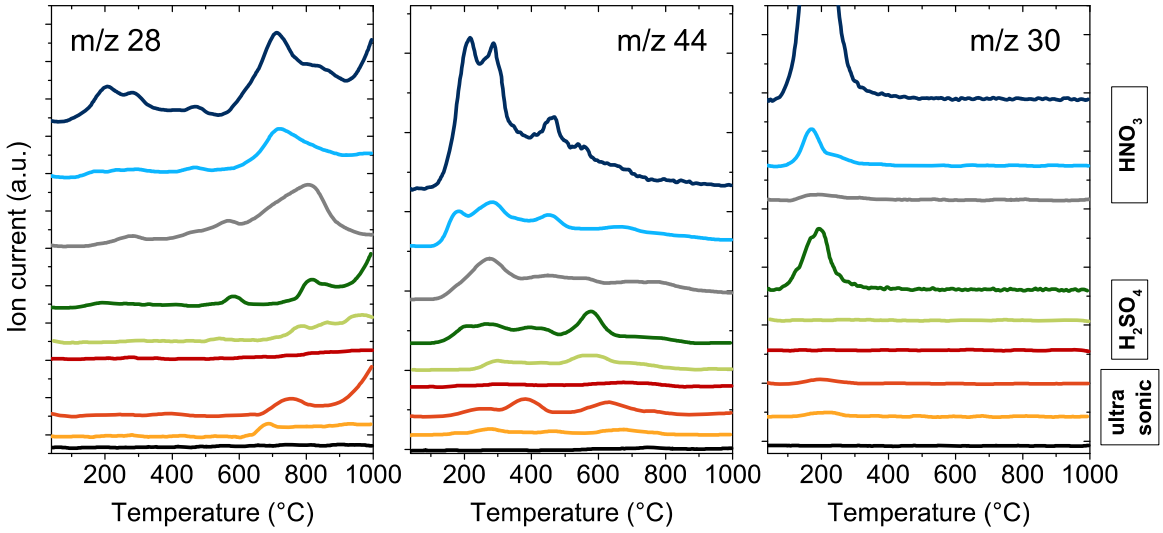

Figure 8. MS signals of thermal analysis of different pre-treated MWCNT (black: ultra-sonic; red: H_2SO_4; grey: HNO_3) and corresponding manganese loaded samples (light colour: 2wt%; dark color: 6wt%)

XRD measurements show the typical patterns of MWCNT (Figure 9). Differences in intensities can be induced by absorbance effects, while the increase of background with increasing amount of manganese results from fluorescence effects. The manganese loaded XRD patterns show additional reflexes, which can be correlated to mainly MnO_2 ε-Akhtenskite (PDF 89-5171), MnO_2 β-Pyrolusite (PDF 81-2261) and Mn_2O_3 Bixbyite (PDF 89-2809). This insight confirms the results from elemental analysis that different Mn_yO_x species are present. There is no difference observable in the XRD patterns between the applied pre-treatment methods.

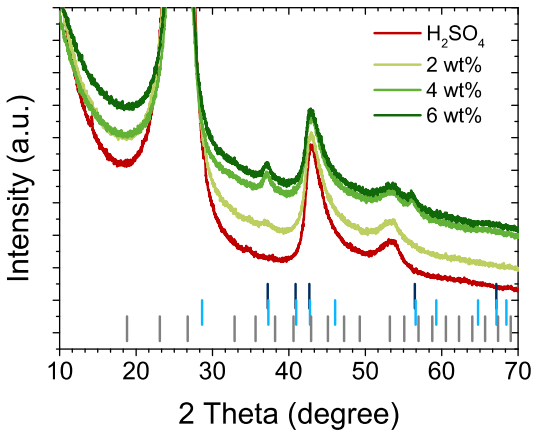

Figure 9. XRD patterns of H_2SO_4 pre-treated MWCNT and corresponding impregnated samples.

Vertical bars representing Bragg reflex positions of MnO_2 ε-Akhtenskite (PDF 89-5171, blue), MnO_2 β-Pyrolusite (PDF 81-2261, light blue), and Mn_2O_3 Bixbyite (PDF 89-2809, grey). XRD patterns of HNO_3 pre-treated samples look alike.

Regarding the fingerprint region of the Raman spectra it is possible to determine different phases of manganese species. It is possible to detect different manganese oxide phases (Figure 10). In comparison to literature the samples contain different Mn_3O_4, MnO_2, Mn_3O_4, and Mn_2O_3 species [25,26]. Considering that the applied laser wavelength influences the spectra immense [27] and different wavelengths were applied it is difficult to distinguish between the different manganese oxide compositions. In addition to this, the MWCNT perform a high background. With increasing amount of deposited manganese oxides the background of the Raman spectra increases furthermore due to fluorescence effects. The applied XRD and Raman methods reveal that various manganese oxides are present, significant differences between the different pre-treated samples could not be determined. The acid treatment and surface functionalization lead to a partial amorphization of the tube walls (Figure 11a). In case of H_2SO_4, the amorphization is less pronounced and occurs mainly at defects in the structure of the tubes, while graphitic and well crystalline regions do not show any degradation. In the HAADF images (Figure 10b, c), manganese atoms and clusters show up as bright spots due to their higher atomic number. Manganese is found to be located at the edges on the surface of the MWCNT pre-treated with nitric acid whereas these stabilizing edges are missing on the surface of the H_2SO_4 pre-treated sample. Therefore manganese is distributed unspecific among the powder sample. Additionally to the small manganese clusters on the surface, manganese oxide particles are situated among the MWCNT when loaded with more than 4 wt% of manganese.

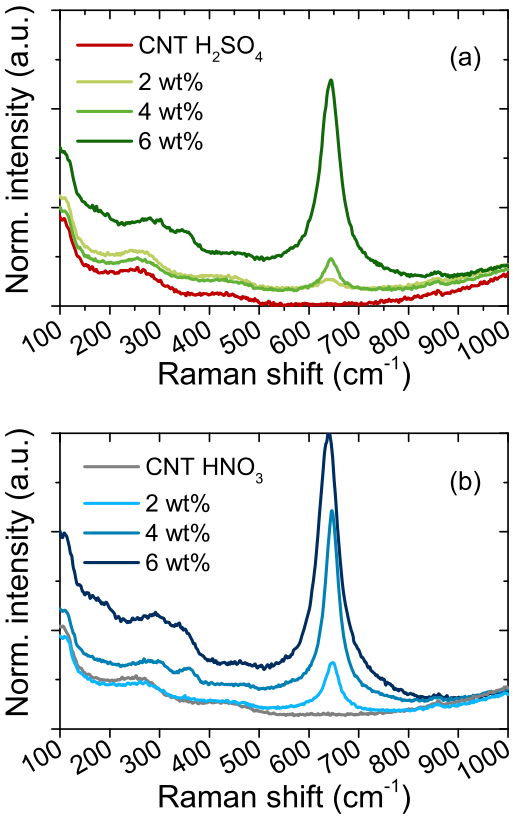

Figure 10. Raman spectra of the sulfuric (a) and nitric acid (b) pre-treated samples loaded with increasing amounts of manganese oxides. The shift of the background with increasing amount of deposited manganese results from fluorescence effects.

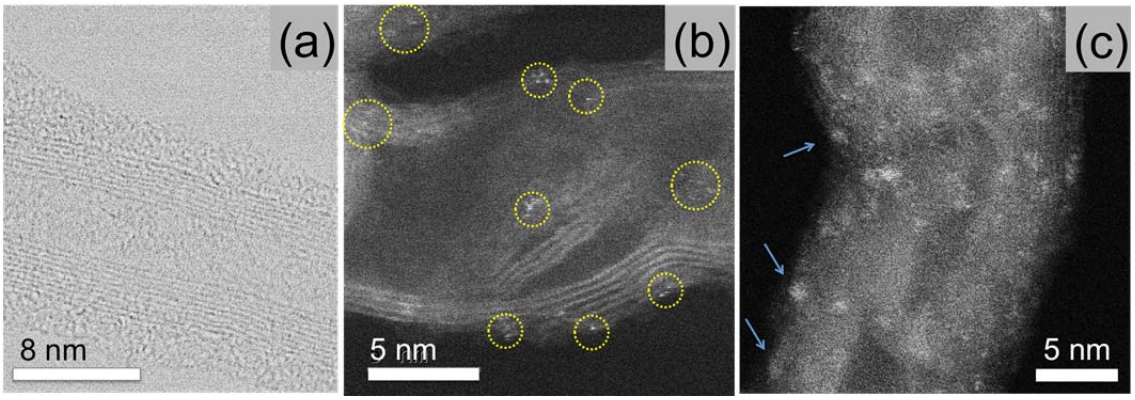

Figure 11. Amorphization of the outer walls of MWCNT after acidic pre-treatment (a). Microscopy images of sulfuric (b) and nitric acid (c) pre-treated MWCNT loaded with 6wt% of manganese.

Zeta potential measurements were performed for the different pre-treated MWCNT loaded with

manganese. In accordance to Raman spectroscopy and TG-MS analysis the Zeta potential of the nitric acid treated sample is much more negative due to the functional groups on the surface than the sulfuric acid and the ultra-sonic bath pre-treated samples. The deposition of manganese increases the zeta potential to even more negative values in comparison to non-loaded MWCNT, caused by the formation of oxyhydroxides from redox processes as known from literature (Figure 12) [28]. Manganese oxide transformations are exposed by pH values, correlated with a subsequent change of pk_s values that area ware from Pourbaix diagrams. This effect is visible for the samples pre-treated with sulfuric acid and ultra-sonic bath at around pH 8. In the low pH-range the zeta potentials of the initially manganese loaded samples follow the trend of the supporting pre-functionalized MWCNT as if the manganese oxides are washed out. This trend is observable for the ultra-sonic bath as well for the sulfuric acid treated samples concluding that there are no stabilizing effects for the samples without craters and edges on the surface. H_2SO_4 pre-treated samples contain functional groups on the surface that could serve as anchoring sites but these samples behave similar to the samples pre-treated in an ultra-sonic bath containing no functional groups. Solely the pH value where dissolving takes place is shifted a little bit from around pH 8 to 7 for the sulfuric acid treated samples due to weak stabilization by the functional groups.

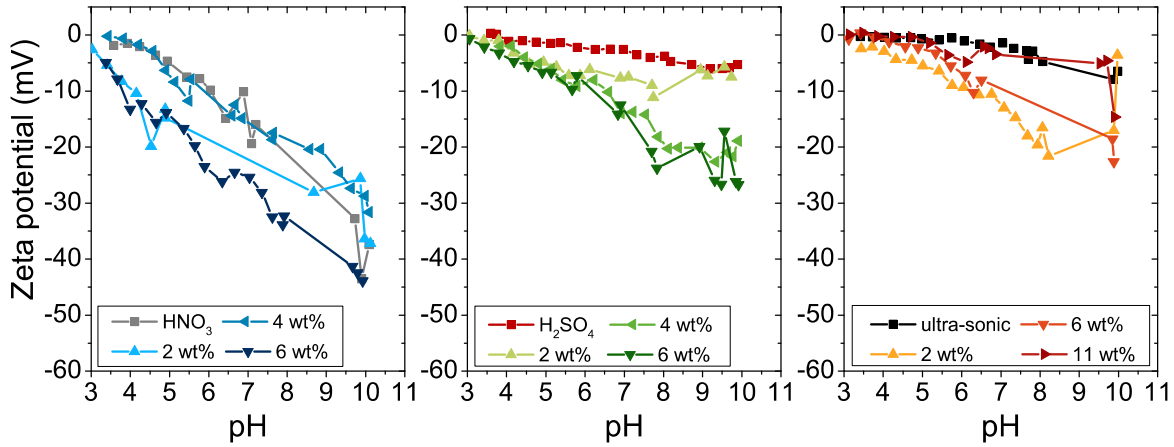

Figure 12. Zeta potentials of manganese deposited samples on nitric acid (left) sulfuric acid (middle) and ultra-sonic (right) pre-treated samples.

4. Conclusions

Treatment of carbon nanotubes with sulfuric or nitric acid has a specific influence on the formation of functional groups on the surface. There are significant amounts of carboxylic acid, lactone and anhydride

groups formed with nitric acid while only minor functional groups are present for H_2SO_4, determined by thermal analysis, and Raman fitting procedure. Craters and edges characterize the surface of the nitric acid pre-treated samples formed by discontinuity of the graphene layers. The outer graphene layers of the H_2SO_4 pre-treated MWCNT stay mainly intact although there is an evident amount of functional groups formed on the surface. It was shown that the texture of the MWCNT is responsible for the stabilization of the deposited manganese. Functional groups on the surface play only a minor role when manganese is deposited by a precipitation mechanism. The precipitation loading mechanism led to the formation of small manganese oxide particle when exceeding a loading amount of 4 wt%. The formation of various manganese oxides could be observed by the applied Raman spectroscopy and XRD measurements. The synthesized materials are precursor for potential Mn-oxide electrocatalysts and have to be further transferred into an active form by calcination in a careful way.

Acknowledgments

The authors would like to thank Prof. Dr. Lehmann from Max-Planck-Institut Für Kohlenforschung to provide access to the microscopy devices. Sincere thanks for measurements and support are given to Maike Hashagen for sorption and Frank Girgsdies for XRD measurements. We thank Birgit Deckers for graphical support. The Max-Planck-Gesellschaft is thanked for realization of the project.

References:

[1] Dau, H., Limberg, C., Reier, T., Risch, M., Roggan, S., Strasser, P., Chemcatchem 2, (2010) 724.
[2] Ortel, E., Reier, T., Strasser, P., Kraehnert, R., Chemistry of Materials 23, (2011) 3201.
[3] Mette, K., Bergmann, A., Tessonnier, J.-P., Haevecker, M., Yao, L., Ressler, T., Schloegl, R., Strasser, P., Behrens, M., ChemCatChem 4, (2012) 851.
[4] Serp, P., Corrias, M., Kalck, P., Applied Catalysis a-General 253, (2003) 337.
[5] Endo, M., Strano, M. S., Ajayan, P. M., Carbon Nanotubes 111, (2008) 13.
[6] Tasis, D., Tagmatarchis, N., Bianco, A., Prato, M., Chemical Reviews 106, (2006) 1105.
[7] Tian, G.-L., Zhang, Q., Zhang, B., Jin, Y.-G., Huang, J.-Q., Su, D. S., Wei, F., Advanced Functional Materials 24, (2014) 5956.
[8] Jansen, R. J. J., Vanbekkum, H., Carbon 32, (1994) 1507.
[9] Balasubramanian, K., Burghard, M., Small 1, (2005) 180.
[10] Xu, Y.-j., Arrigo, R., Liu, X., Su, D.-s., New Carbon Materials 26, (2011) 57.
[11] Xia, W., Jin, C., Kundu, S., Muhler, M., Carbon 47, (2009) 919.
[12] Figueiredo, J. L., Journal of Materials Chemistry A 1, (2013) 9351.
[13] Arrigo, R., Wrabetz, S., Schuster, M. E., Wang, D., Villa, A., Rosenthal, D., Girsgdies, F., Weinberg, G., Prati, L., Schloegl, R., Su, D. S., Physical Chemistry Chemical Physics 14, (2012) 10523.

[14] Figueiredo, J. L., Pereira, M. F. R., Freitas, M. M. A., Orfao, J. J. M., Carbon 37, (1999) 1379.
[15] Meng, Y., Song, W., Huang, H., Ren, Z., Chen, S.-Y., Suib, S. L., Journal of the American Chemical Society 136, (2014) 11452.
[16] Gao, M.-R., Xu, Y.-F., Jiang, J., Zheng, Y.-R., Yu, S.-H., Journal of the American Chemical Society 134, (2012) 2930.
[17] [17] Huang, H. J., Zhang, W. Y., Fu, Y. S., Wang, X., Electrochimica Acta 152, (2015) 480.
[18] Zhang, Y., Yao, Q. Q., Gao, H. L., Zhang, L. S., Wang, L. Z., Zhang, A. Q., Song, Y. H., Wang, L. X., J. Anal. Appl. Pyrolysis 111, (2015) 233.
[19] Yan, J., Fan, Z., Wei, T., Qian, W., Zhang, M., Wei, F., Carbon 48, (2010) 3825.
[20] Rinaldi, A., Frank, B., Su, D. S., Hamid, S. B. A., Schloegl, R., Chem. Mater. 23, (2011) 926.
[21] Tessonnier, J.-P., Ersen, O., Weinberg, G., Pham-Huu, C., Su, D. S., Schloegl, R., Acs Nano 3, (2009) 2081.
[22] Tscharnuter, W. W., Applied Optics 40, (2001) 3995.
[23] Düngen, P., Prenzel, M., Pfänder, N., Buller, S., Schlögl, R., submitted (2015)
[24] Frank, B., Rinaldi, A., Blume, R., Schloegl, R., Su, D. S., Chemistry of Materials 22, (2010) 4462.
[25] Julien, C. M., Massot, M., Poinsignon, C., Spectrochimica Acta Part a-Molecular and Biomolecular Spectroscopy 60, (2004) 689.
[26] Kapteijn, F., Vanlangeveld, A. D., Moulijn, J. A., Andreini, A., Vuurman, M. A., Turek, A. M., Jehng, J. M., Wachs, I. E., Journal of Catalysis 150, (1994) 94.
[27] Buciuman, F., Patcas, F., Craciun, R., Zahn, D. R. T., Physical Chemistry Chemical Physics 1, (1999) 185.
[28] Hem, J. D., Chemical Geology 21, (1978) 199.